

Contrastive Learning and Adversarial Disentanglement for Task-Oriented Semantic Communications

Omar Erak, Omar Alhussein, *Member, IEEE*, Wen Tong, *Fellow, IEEE*

Abstract—Task-oriented semantic communication systems have emerged as a promising approach to achieving efficient and intelligent data transmission, where only information relevant to a specific task is communicated. However, existing methods struggle to fully disentangle task-relevant and task-irrelevant information, leading to privacy concerns and subpar performance. To address this, we propose an information-bottleneck method, named CLAD (contrastive learning and adversarial disentanglement). CLAD utilizes contrastive learning to effectively capture task-relevant features while employing adversarial disentanglement to discard task-irrelevant information. Additionally, due to the lack of reliable and reproducible methods to gain insight into the informativeness and minimality of the encoded feature vectors, we introduce a new technique to compute the information retention index (IRI), a comparative metric used as a proxy for the mutual information between the encoded features and the input, reflecting the minimality of the encoded features. The IRI quantifies the minimality and informativeness of the encoded feature vectors across different task-oriented communication techniques. Our extensive experiments demonstrate that CLAD outperforms state-of-the-art baselines in terms of semantic extraction, task performance, privacy preservation, and IRI. CLAD achieves a predictive performance improvement of around 2.5-3%, along with a 77-90% reduction in IRI and a 57-76% decrease in adversarial attribute inference attack accuracy.

Index Terms—Contrastive learning, disentangled representation learning, information-bottleneck, semantic communications, task-oriented communications.

I. INTRODUCTION

In conventional communication systems, the primary objective has been to ensure reliable transmission of data, focusing on delivering bit sequences across noisy channels without considering the meaning, context, or purpose of the data being transmitted. Shannon’s mathematical theory of communication focuses on optimizing metrics such as data rate, error rate, and bandwidth efficiency, whilst being agnostic to the ultimate purpose and relevance of the transmitted information [1]. This approach has been widely successful and effective for general communication needs thus far. However, next-generation communication systems, beginning with 6G, require more intelligent and task-aware communication methods to enable emerging applications [2], [3], such as computer vision [4], autonomous driving [5], extended reality (XR) [6], and generative artificial intelligence (AI) [7].

Omar Erak and Omar Alhussein are with the KU 6G Research Center, Department of Computer Science, Khalifa University, Abu Dhabi, UAE (e-mail: omarerak@ieee.org, omar.alhussein@ku.ac.ae).

Wen Tong is with the Huawei Wireless Research, Wireless Advanced System and Competency Centre, Huawei Technologies Co. Ltd., Ottawa, ON K2K 3J1, Canada, (e-mail: tongwen@huawei.com).

As we move towards these advanced systems, there is a growing recognition that communication should not merely be about transmitting raw data, but about understanding and leveraging the underlying meaning and purpose of the data. This shift towards task-oriented semantic communications represents a fundamental change in the design of communication networks [8], [9]. Instead of focusing solely on the accurate and efficient transmission of bits, these new approaches aim to ensure that the information most relevant to the specific task or decision-making process is prioritized and delivered with minimal delay. For example, in a smart city environment [10], rather than transmitting all sensor data from traffic cameras, task-oriented communications focuses on sending only the information necessary to identify and respond to potential hazards or optimize traffic flow in real time.

With the growing success and popularity of deep learning (DL) in various wireless communication applications [11], [12], many emerging task-oriented communication systems have adopted DL approaches to encode task-relevant information to improve task performance and efficiency of the communication system [13]–[15]. Nevertheless, most proposed schemes do not focus quantifying or benchmarking the amount of information that the encoded features retain about the input, primarily due to the computational difficulty of estimating mutual information and the lack of a unified methodology that provides fair and reproducible results. This omission is critical, as understanding the mutual information is key to developing systems with improved bandwidth and latency. Moreover, there has been little emphasis on explicitly discarding task-irrelevant information, often leading to a trade-off between task performance and information compression.

Furthermore, most current approaches rely on maximizing mutual information between the encoded features and the target using variational approximations based on the cross-entropy loss [13], [15], [16]. However, deriving a maximization for the mutual information between the encoded feature vector and the targets based on contrastive learning [17] remains unexplored for task-oriented communication systems.

To address the aforementioned challenges, we develop a task-oriented communication system based on contrastive learning [17] and disentangled representation learning [18] and we devise a new metric to compute comparative values for a proxy of mutual information between the encoded features and the inputs across different systems, rather than computing the exact mutual information. More specifically, our major contributions are as follows:

- We derive a lower bound for the mutual information between the encoded features and the target using con-

trastive learning principles. We show that the contrastive learning based lower bound improves task accuracy and performance compared to the traditional cross-entropy based mutual information approximations;

- We propose a systematic training methodology based on an innovative loss function, designed to extract task-irrelevant information through reconstruction losses while disentangling it from task-relevant features using adversarial methods. This enables the system to prioritize the transmission of task-relevant features while minimizing communication overhead and reducing unnecessary information transmission;
- To address the current limitation of lacking a reliable and unified approach for estimating the mutual information between the encoded features and input data, we introduce a new metric named the information retention index (IRI) which serves as a proxy for the mutual information. This metric compares the informativeness and minimality of the encoded features across various task-oriented communication methods, providing deeper insights into system behavior and enabling a more rigorous comparison of their performance;
- We evaluate our proposed task-oriented communication system in diverse channel conditions. It is tested against several existing task-oriented communication methods, demonstrating improved task performance, enhanced privacy awareness, and reduced amount of stored information across a wide range of transmission scenarios.

The rest of this paper is organized as follows. In Section II, we provide an overview of related works in task-oriented communications, contrastive learning, and disentangled representation learning. Section III introduces the system model followed by an in-depth discussion of the problem statement and involved challenges. Section V discusses our proposed method (CLAD) and the associated mathematical formulations and algorithms. In Section VI, we outline our experimental setup, and provide a thorough analysis and discussion of the results and their implications. Finally, Section VII concludes the paper with a discussion on the importance of our results as well as future work and possibilities in the realm of task-oriented semantic communications.

II. RELATED WORK

DL-based communication systems have shown success in recent years. DeepJSCC (Deep Joint Source-Channel Coding) is a recent advancement in the field of wireless communications that utilizes deep learning to jointly optimize source and channel coding, which are traditionally treated as separate tasks [14]. Unlike conventional methods that rely on separate compression and error-correction codes, DeepJSCC uses neural networks to directly map source data to channel symbols, allowing for an end-to-end optimization of the communication system. DeepJSCC can be trained on a classification task by minimizing the cross-entropy loss, ensuring task-specific performance; however, it does not inherently ensure that only task-relevant features are transmitted.

Building on that, Shao et al. [13] proposed a task-oriented communication system for edge inference by leveraging the in-

formation bottleneck (IB) theory [19], and variational approximations [16] to balance a trade-off between the minimality of the transmitted feature vector and the task performance. Their results demonstrate improved latency and classification accuracy. Another work focuses on improving the aforementioned IB framework for task-oriented communication systems by introducing an information bottleneck framework that ensures robustness to varying channel conditions [15].

Wang et al. formulate a privacy-utility trade-off to develop an IB-based privacy-preserving task-oriented communication system against model inversion attacks [20]. This is achieved by striking a balance between the traditional IB-based loss functions similar to the work discussed above and a mean squared error (MSE) based term that aims at maximizing reconstruction distortion. Their results demonstrate improved privacy with minimal impact to task performance.

Despite the successful results achieved by the aforementioned task-oriented communication systems, there remain several key areas that warrant further investigation and improvement. One significant limitation in the existing literature is the lack of results and comprehensive benchmarking on the mutual information between the encoded features and the input, given a particular task-oriented communication system. In task-oriented communication systems, mutual information plays a critical role in determining the efficiency of the system, particularly regarding the preservation of information during transmission.

Furthermore, while task-specific performance, specifically classification accuracy, has been improved by these advancements, there is still room for enhancing performance further. Another key challenge in these systems is balancing multiple trade-offs, such as task performance, informativeness, minimality and privacy. These trade-offs are typically managed through careful tuning of hyperparameters. Reducing the dependency on hyperparameters would make these systems more robust and easier to deploy in real-world scenarios.

Contrastive learning has gained significant attention in recent years, particularly for its success in unsupervised learning [17], [21]–[23]. By leveraging the concept of instance discrimination, contrastive learning methods aim to pull together positive pairs for example, augmentations of the same image, while pushing apart negative pairs for example, different images, thus learning meaningful representations of data without the need for labels. More recently, contrastive learning has also shown exceptional results in supervised learning scenarios. By incorporating label information into the contrastive loss function, methods such as supervised contrastive learning (SupCon) [24] have improved upon traditional cross-entropy loss. Contrastive learning has not been investigated for task-oriented communication systems as an alternative to cross-entropy based mutual information approximation techniques.

Disentangled representation learning has been widely studied in recent years. Prominent examples include the β -VAE [25], that extends the variational autoencoder (VAE) by introducing a regularization term that encourages disentanglement, and FactorVAE [26], that further improves this disentanglement by encouraging the representations' distribution to be factorial and therefore independent across the dimen-

sions. Other works [27]–[29], explored disentangling through adversarial-based objectives [30].

III. SYSTEM MODEL AND NOTATIONS

A. Notations

Throughout this paper, we use the following notational conventions. Random variables are denoted by uppercase letters, such as X , Y , and Z . Their corresponding realizations (i.e., specific instances) are denoted by lowercase bold letters, such as \mathbf{x} , \mathbf{y} , and \mathbf{z} . The space from which these random variables are drawn is represented by calligraphic letters, such as \mathcal{X} , \mathcal{Y} and \mathcal{Z} . We denote entropy of a random variable X by $H(X)$. The mutual information between two random variables X and Y , is denoted by $I(X; Y)$. We use $I(Z; X|Y)$ to denote the conditional mutual information between Z and X given Y . We use the expectation notation $\mathbb{E}[\cdot]$, which refers to the average value of a random variable over a distribution.

B. System Model

We consider a communication system with a transmitter that includes a feature extractor and a joint source-channel coding (JSCC) encoder. We collectively refer to these components as the task-relevant encoder (TRE). The TRE encodes an input image $\mathbf{x} \in \mathcal{X}$ into a lower-dimensional feature vector $\mathbf{z} \in \mathcal{Z}$. Encoded vector \mathbf{z} is then transmitted to a receiver over a noisy wireless channel. The primary objective is to transmit a minimal yet informative representation (\mathbf{z}), by discarding task-irrelevant information while ensuring that \mathbf{z} contains only the essential information for accurate downstream classification at the receiver.

The overall transmission and decoding process can be described by the following Markov chain:

$$Y \rightarrow X \rightarrow Z \rightarrow \hat{Z} \rightarrow \hat{Y}, \quad (1)$$

where X is the random variable representing the input images, Z is the random variable representing the encoded feature vectors, \hat{Z} is the noisy signals received by the receiver, Y is the random variable representing the labels of the input images, and \hat{Y} is the random variable representing the predicted labels at the receiver.

At the transmitter, the TRE encodes input image $\mathbf{x} \in \mathbb{R}^N$, where N represents the number of pixels in the image (Height \times Width \times Color Channels). The encoder maps this input into a lower-dimensional feature vector $\mathbf{z} \in \mathbb{R}^d$, where d is the dimension of the encoded feature vector. The encoding function, denoted by $f_\theta : \mathbb{R}^N \rightarrow \mathbb{R}^d$, is parameterized by θ , and the encoding process can be expressed as

$$\mathbf{z} = f_\theta(\mathbf{x}) \quad (2)$$

Feature vector \mathbf{z} is then prepared for transmission over the wireless channel by being mapped to channel input symbols. The role of the TRE is twofold: encoding the input data into feature representations and preparing them as channel symbols suitable for transmission. The encoded feature vector $\mathbf{z} \in \mathbb{R}^d$ is transmitted over a wireless channel, which is modeled as an additive white Gaussian noise (AWGN) channel. The channel

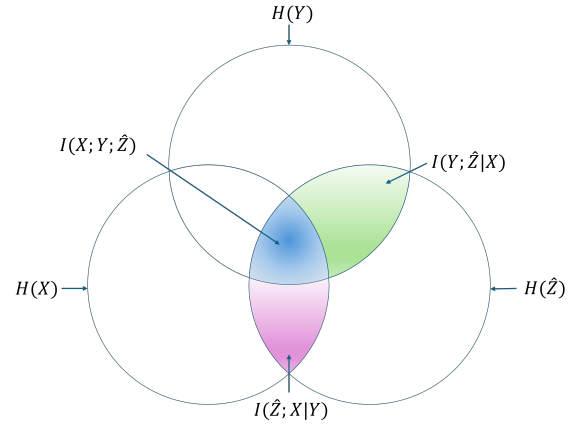


Figure 1. Information diagram for three random variables X , Y , \hat{Z} . The union of the blue and pink regions yields $I(\hat{Z}; X)$, and the union of the blue and green regions yields $I(\hat{Z}; Y)$.

introduces noise and distortion, and the received signal $\hat{\mathbf{z}} \in \mathbb{R}^d$ at the receiver is expressed as

$$\hat{\mathbf{z}} = \mathbf{z} + \mathbf{n}, \quad (3)$$

where $\mathbf{n} \sim \mathcal{N}(0, \sigma^2 \mathbf{I})$ is the additive Gaussian noise with variance σ^2 . The noise variance σ^2 is related to the channel's *signal-to-noise ratio* (SNR), which quantifies the channel quality. The SNR in decibels (dB) is given by

$$\text{SNR}_{\text{dB}} = 10 \log_{10} \left(\frac{\mathbb{E}[\|\mathbf{z}\|^2]}{\sigma^2} \right). \quad (4)$$

At the receiver, a classifier, denoted by $q_\phi : \mathbb{R}^d \rightarrow \mathbb{R}^M$, where M is the number of labels, is parameterized by ϕ . The classifier maps the received noisy signal $\hat{\mathbf{z}}$ to predicted label $\hat{\mathbf{y}} \in \mathbb{R}^M$ as

$$\hat{\mathbf{y}} = q_\phi(\hat{\mathbf{z}}). \quad (5)$$

The classifier is trained to minimize the loss between the predicted label ($\hat{\mathbf{y}}$) and the true label (\mathbf{y}). Since true posterior distribution $p(\mathbf{y}|\hat{\mathbf{z}})$ is intractable, q_ϕ serves as an approximation based on the received noisy signal.

IV. PROBLEM DESCRIPTION

In this section, we identify the primary challenges that arise when transmitting features over a communication channel and utilizing them for a downstream classification task. Our goal is to ensure that the transmitted features contain only the minimum necessary information required for the downstream task to maximize efficiency whilst being privacy aware. Furthermore, we argue that it is necessary to have a fair, reproducible, and unified method to obtain comparative values that act as a proxy for mutual information between the encoded features and the input data to allow effective benchmarking of different task-oriented communication systems.

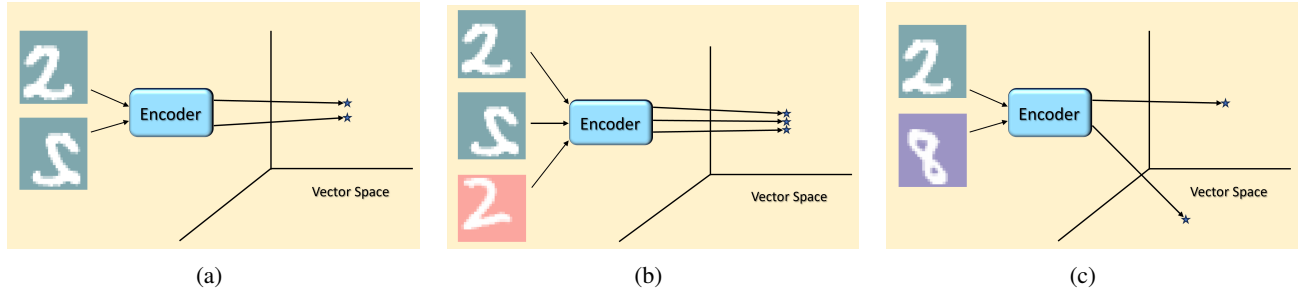


Figure 2. (a): Self-supervised contrastive learning: The model works only on augmentations of the same image; (b): Supervised contrastive learning: Label information is used to align similar classes in vector space; and (c) Both self-supervised and supervised contrastive learning push apart different images in the vector space.

A. Minimum Necessary Information

Following [31], the Minimum Necessary Information (MNI) criterion for an ideal representation \hat{Z} under ideal transmission conditions must satisfy the following key principles:

- **Informativeness:** Representation \hat{Z} should contain all the necessary information to predict Y , requiring us to maximize the mutual information $I(\hat{Z}; Y)$.
- **Necessity:** Representation \hat{Z} should contain the necessary amount of information in order to perform well in the downstream task, any less information would mean that Z has discarded task-relevant information. Necessity can be defined as

$$I(X; Y) \leq I(Y; \hat{Z}) \quad (6)$$

- **Minimality:** Among all possible representations Z that satisfy the task of predicting Y , we seek the one that encodes the least amount of information about X beyond what is strictly necessary for the task. This can be formulated as

$$\min_{\hat{Z}} I(\hat{Z}; X) \quad \text{subject to} \quad I(X; Y) = I(\hat{Z}; Y) \quad (7)$$

Any more information than that would result in Z having redundant information about X that is unnecessary for predicting Y .

Given the above we conclude that in an optimal case under ideal channel conditions we must have

$$I(\hat{Z}; X) = I(\hat{Z}; Y) = I(X; Y), \quad (8)$$

this implies that \hat{Z} contains exactly the amount of information necessary to perform the task of predicting Y from X , no more and no less. At the MNI point, \hat{Z} captures all the relevant information needed for the task, while discarding any irrelevant or redundant information about X .

B. Privacy Concerns and Task-Irrelevant Information

The second challenge is privacy concerns due to the leakage of task-irrelevant information from X into \hat{Z} . If \hat{Z} retains information about X that is not relevant to predicting Y , this may inadvertently expose sensitive or private data, and could make the system more vulnerable to different attacks such as attribute inference attacks and model inversion attacks [32], [20]. Therefore, disentangling task-irrelevant information

ensures that \hat{Z} does not encode unnecessary or sensitive information that is not directly relevant to the downstream task, which minimizes privacy risks.

C. Quantifying Information Retention

In task-oriented communication systems, it is critical to have an understanding of the mutual information $I(\hat{Z}; X)$ as it provides insights into how much of the original input information X is encoded in \hat{Z} and can directly affect latency, bandwidth and privacy. However, a significant challenge arises because the estimation of $I(\hat{Z}; X)$ varies drastically depending on the estimation method used. Indeed, multiple works have reported widely different $I(\hat{Z}; X)$ for the same task-oriented approach [16], [28]. This makes it difficult to arrive at reliable conclusions about the amount of information being retained in \hat{Z} .

Given these discrepancies, we argue that it is crucial to devise a method that yields consistent, reliable and fair comparative estimates of information retention, even if the exact value of $I(\hat{Z}; X)$ is intractable. Instead of absolute precision, a method that provides relative and comparable estimates across different systems would greatly enhance the ability to evaluate and optimize different task-oriented communication systems.

D. Limitations of Variational Information Bottleneck (VIB)

The variational information bottleneck (VIB) has been the de facto method for many task-oriented communication systems. VIB tries to minimize the following objective:

$$\mathcal{L}_{\text{VIB}} = \beta I(\hat{Z}; X) - I(\hat{Z}; Y), \quad (9)$$

where $I(\hat{Z}; X)$ measures the amount of information retained from the input X , and $I(\hat{Z}; Y)$ represents the informativeness of Z for predicting Y . Hyperparameter β controls the trade-off between preserving task-relevant information and discarding irrelevant information. To maximize $I(\hat{Z}; Y)$, a cross-entropy based loss is used, and the Kullback–Leibler divergence is used to minimize $I(\hat{Z}; X)$ [13], [15], [16].

However, VIB-based task-oriented communication systems presents several challenges:

- **Limitation of cross-entropy based loss:** The majority of task-oriented communication systems rely on the cross-entropy loss as a variational approximation to maximize

$I(\hat{Z}; Y)$. However, it has been shown recently that supervised contrastive learning based loss [24] outperforms the cross-entropy loss in different settings.

- **Conflicting objectives:** The VIB objective which maximizes $I(\hat{Z}; X)$ and minimizes $I(\hat{Z}; Y)$ leads to a conflicting objective [31]. If we consider the information diagram [33] presented in Fig. 1, it is evident that the region shaded in blue, namely $I(X; Y; \hat{Z})$ is a subset of $I(\hat{Z}; X)$ and $I(\hat{Z}; Y)$ and is therefore maximized and minimized simultaneously.
- **Inadequate disentanglement:** VIB does not explicitly enforce a separation between the portions of Z that are relevant for predicting Y and those that capture irrelevant or redundant details from X . This lack of disentanglement can compromise the privacy and efficiency of the transmitted representation.

V. PROPOSED METHOD: CLAD

The core idea of CLAD is to create an end-to-end communication system that explicitly learns to disentangle task-relevant information from task-irrelevant content, enabling both high task accuracy and improved privacy. Rather than simply combining existing techniques, CLAD integrates supervised contrastive learning, adversarial training, and reconstruction-based supervision into a unified, structured framework that aligns with the Minimum Necessary Information (MNI) principle.

Each component in CLAD is designed to target a specific challenge:

- **Contrastive learning** maximizes the informativeness of the representation with respect to the downstream task.
- **Adversarial disentanglement** promotes independence between task-relevant and irrelevant features, suppressing information leakage.
- **Reconstruction learning** ensures that task-irrelevant features are adequately captured.

To ensure effective optimization, CLAD adopts a *three-stage training strategy*, where each stage isolates and refines a different component of the system. This design is intentional — it prevents interference between competing objectives, stabilizes training, and encourages modular reuse of the encoders across stages.

CLAD utilizes two key encoders: the TRE, which maps the input into the task-relevant channel codeword Z_1 , and the task-irrelevant encoder (TIE), which maps the input into task-irrelevant channel codeword Z_2 . The task performance is optimized through contrastive learning, which aims to maximize the mutual information $I(\hat{Z}_1; Y)$, ensuring that \hat{Z}_1 captures the most informative features for downstream classification. The disentanglement is achieved through reconstruction learning to capture task-irrelevant information in \hat{Z}_2 , and adversarial training is utilized to minimize the mutual information $I(\hat{Z}_1; \hat{Z}_2)$, thus promoting independence between the two feature representations. The different components and training stages of CLAD are visualized in Fig. 3. These components are optimized together to ensure both high task accuracy and effective disentanglement of information, corresponding to the following maximization objective:

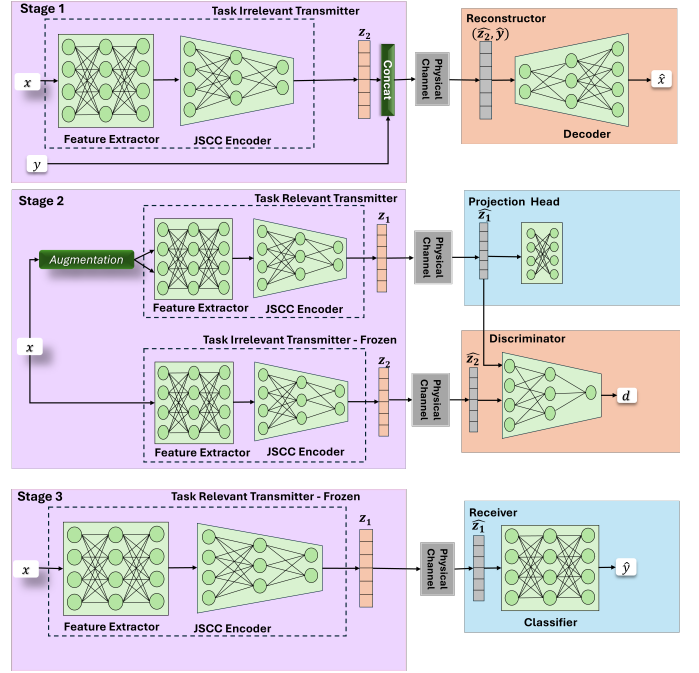


Figure 3. Three stages for training CLAD

$$\mathcal{L}_{\text{CLAD}} = I(\hat{Z}_1; Y) + I(\hat{Z}_2; X|Y) - I(\hat{Z}_1; \hat{Z}_2). \quad (10)$$

Here, the objective consists of three key terms:

- $I(\hat{Z}_1; Y)$ maximizes the mutual information between task-relevant features \hat{Z}_1 and the label Y using contrastive learning;
- $I(\hat{Z}_2; X|Y)$ ensures that \hat{Z}_2 captures the residual information in X that is not covered by Y by utilizing a reconstruction loss;
- $I(\hat{Z}_1; \hat{Z}_2)$ minimizes the information overlap between \hat{Z}_1 and \hat{Z}_2 , encouraging disentanglement via an adversarial loss.

Reflecting back on Fig. 1, we can see that our new objective maximizes the blue region (task-relevant information) and minimizes the pink region (task-irrelevant information) and avoids the conflicting objectives of VIB. We explain each of the components of our loss function in detail below, accompanied by their mathematical formulations, implementation details, and training strategy.

A. Contrastive Loss for Task-Relevant Features

To maximize $I(\hat{Z}_1; Y)$, we adopt a supervised contrastive learning framework similar to [24]. First, we apply an augmentation function, which applies different augmentations such as cropping, rotating and reflecting, $\text{Aug}(\cdot)$ to the input image \mathbf{x} to generate two different views $\tilde{\mathbf{x}}_1 = \text{Aug}(\mathbf{x})$ and $\tilde{\mathbf{x}}_2 = \text{Aug}(\mathbf{x})$. These augmented samples are then passed through the TRE, denoted by $f_\theta(\cdot)$, resulting in two representations, $\mathbf{z}_1 = f_\theta(\tilde{\mathbf{x}}_1)$ and $\mathbf{z}_2 = f_\theta(\tilde{\mathbf{x}}_2)$, where $\mathbf{z} \in \mathbb{R}^d$.

Following that, these representations are transmitted over the physical channel and projected into a lower-dimensional space through a projection head, $h_\psi(\cdot)$ parameterized by ψ ,

Algorithm 1 Stage 1: Train Task-Irrelevant Encoder with Reconstructor

Input: \mathcal{X}_{train} (Training dataset), κ (SNR), λ (Learning rate)

Output: Frozen task-irrelevant encoder g_η

- 1: Initialize η, ω
 - 2: **while** not converged **do**
 - 3: Sample $(\mathbf{x}, \mathbf{y}) \sim \mathcal{X}_{train}$
 - 4: $\mathbf{z}_2 \leftarrow g_\eta(\mathbf{x})$
 - 5: $\mathbf{n} \sim \mathcal{N}(0, \sigma^2 \mathbf{I}), \sigma^2 \leftarrow \frac{\mathbb{E}[\|\mathbf{z}_2\|^2]}{10^{10}}$
 - 6: $\hat{\mathbf{z}}_2 \leftarrow \mathbf{z}_2 + \mathbf{n}$
 - 7: $\hat{\mathbf{x}} \leftarrow r_\omega(\hat{\mathbf{z}}_2, \mathbf{y})$
 - 8: $\mathcal{L}_{recon} \leftarrow \|\mathbf{x} - \hat{\mathbf{x}}\|^2$
 - 9: $\eta \leftarrow \eta - \lambda \nabla_\eta \mathcal{L}_{recon}$
 - 10: $\omega \leftarrow \omega - \lambda \nabla_\omega \mathcal{L}_{recon}$
 - 11: **end while**
 - 12: Discard r_ω
 - 13: Freeze η
-

yielding $\mathbf{h}_1 = h_\psi(\hat{\mathbf{z}}_1)$ and $\mathbf{h}_2 = h_\psi(\hat{\mathbf{z}}_2)$, where $\mathbf{h} \in \mathbb{R}^{d_p}$, and d_p represents the dimensionality of the projection space.

A contrastive loss, $\mathcal{L}_{contrast}$, is designed to maximize the agreement between representations of similar class samples while minimizing the similarity between representations of different class samples. Considering a batch of intermediate features $[\mathbf{z}_1, \dots, \mathbf{z}_B]$ and their corresponding labels $[\mathbf{y}_1, \dots, \mathbf{y}_B]$, the loss function is defined as

$$S_{ij} = \frac{\exp(\mathbf{h}_i^\top \mathbf{h}_j / \tau)}{\sum_{k=1}^B \mathbb{1}_{i \neq k} \exp(\mathbf{h}_i^\top \mathbf{h}_k / \tau)}, \quad (11)$$

$$\mathcal{L}_{contrast} = -\frac{1}{\sum_{i \neq j} \mathbb{1}_{y_i = y_j}} \sum_{i \neq j} \mathbb{1}_{y_i = y_j} \log S_{ij}, \quad (12)$$

where S_{ij} represents the similarity score between the projected representations \mathbf{h}_i and \mathbf{h}_j , τ is a temperature scaling factor, and $\mathbb{1}_{y_i = y_j}$ is an indicator function that equals 1 if $y_i = y_j$ (positive pairs) and 0 otherwise (negative pairs). This loss encourages encoder $f_\theta(\cdot)$ to learn class-discriminative features, ensuring that the latent representation \mathbf{z} captures the necessary information for the downstream classification task.

Next, we prove that minimizing the contrastive loss, defined above, maximizes a lower bound on the task-relevant information $I(\hat{\mathbf{Z}}; Y)$. We begin by considering a simplified situation where we have a query sample \mathbf{h}^+ together with a set $\mathbf{H} = \{\mathbf{h}_1, \dots, \mathbf{h}_B\}$ consisting of B samples. In this set, one sample \mathbf{h}^P is a positive sample from the same class as \mathbf{h}^+ , while the other negative samples are randomly sampled. Namely, $\mathbf{H} = \{\mathbf{h}^P\} \cup \mathbf{H}_{neg}$. The expectation of the contrastive loss is given by

$$\mathbb{E}[\mathcal{L}_{contrast}] = \mathbb{E}_{\mathbf{h}^+, \mathbf{H}} \left[-\log \frac{\exp(\mathbf{h}^{+\top} \mathbf{h}^P / \tau)}{\sum_{i=1}^B \exp(\mathbf{h}^{+\top} \mathbf{h}_i / \tau)} \right]. \quad (13)$$

Equation (13) can be viewed as a categorical cross-entropy loss for recognizing the positive sample \mathbf{h}^P . We define the optimal probability of identifying the positive sample as

$$P(\mathbf{h}_i | \mathbf{H}) = \frac{p(\mathbf{h}_i | y) \prod_{l \neq i} p(\mathbf{h}_l)}{\sum_{j=1}^B p(\mathbf{h}_j | y) \prod_{l \neq j} p(\mathbf{h}_l)} = \frac{\frac{p(\mathbf{h}_i | y)}{p(\mathbf{h}_i)}}{\sum_{j=1}^B \frac{p(\mathbf{h}_j | y)}{p(\mathbf{h}_j)}}. \quad (14)$$

This shows that the optimal value of $\exp(\mathbf{h}^{+\top} \mathbf{h}^P / \tau)$ is $\frac{p(\mathbf{h}^P | y)}{p(\mathbf{h}^P)}$. Assuming that \mathbf{h}^+ is uniformly sampled from all classes, we derive the following bound,

$$\begin{aligned} \mathbb{E}[\mathcal{L}_{contrast}] &\geq \mathbb{E}[\mathcal{L}_{contrast}^{\text{optimal}}] \\ &= \mathbb{E}_{\mathbf{y}, \mathbf{H}} \left[-\log \frac{\frac{p(\mathbf{h}^P | y)}{p(\mathbf{h}^P)}}{\sum_{j=1}^B \frac{p(\mathbf{h}_j | y)}{p(\mathbf{h}_j)}} \right] \\ &= \mathbb{E}_{\mathbf{y}, \mathbf{H}} \left[-\log \frac{\frac{p(\mathbf{h}^P | y)}{p(\mathbf{h}^P)}}{\frac{p(\mathbf{h}^P | y)}{p(\mathbf{h}^P)} + \sum_{\mathbf{h}_j \in \mathbf{H}_{neg}} \frac{p(\mathbf{h}_j | y)}{p(\mathbf{h}_j)}} \right] \\ &= \mathbb{E}_{\mathbf{y}, \mathbf{H}} \left\{ \log \left[1 + \frac{p(\mathbf{h}^P)}{p(\mathbf{h}^P | y)} \sum_{\mathbf{h}_j \in \mathbf{H}_{neg}} \frac{p(\mathbf{h}_j | y)}{p(\mathbf{h}_j)} \right] \right\}. \end{aligned} \quad (15)$$

For large B , from the law of large numbers, we can approximate the sum of negative samples by its expected value as follows,

$$\approx \mathbb{E}_{\mathbf{y}, \mathbf{H}} \left\{ \log \left[1 + \frac{p(\mathbf{h}^P)}{p(\mathbf{h}^P | y)} (B-1) \mathbb{E}_{\mathbf{h}_j \sim p(\mathbf{h}_j)} \frac{p(\mathbf{h}_j | y)}{p(\mathbf{h}_j)} \right] \right\}. \quad (16)$$

Since the negative samples are class-neutral (i.e., independent of y), the inner expectation over negative samples \mathbf{h}_j simplifies to a constant value. This allows us to focus the outer expectation on y and \mathbf{h}^P , concentrating on the probability of correctly identifying the positive sample among the negatives as follows,

$$\begin{aligned} &= \mathbb{E}_{\mathbf{y}, \mathbf{h}^P} \left\{ \log \left[1 + \frac{p(\mathbf{h}^P)}{p(\mathbf{h}^P | y)} (B-1) \right] \right\} \\ &\geq \mathbb{E}_{\mathbf{y}, \mathbf{h}^P} \left\{ \log \left[\frac{p(\mathbf{h}^P)}{p(\mathbf{h}^P | y)} (B-1) \right] \right\} \\ &= \mathbb{E}_{\mathbf{y}, \mathbf{h}^P} \left\{ -\log \left[\frac{p(\mathbf{h}^P | y)}{p(\mathbf{h}^P)} \right] + \log(B-1) \right\} \\ &= -I(\mathbf{h}^P; y) + \log(B-1) \geq -I(\hat{\mathbf{z}}; y) + \log(B-1). \end{aligned} \quad (18)$$

From the above, the last inequality in (18) follows from the data processing inequality [19]. Finally, we conclude that

$$\mathbb{E}[\mathcal{L}_{contrast}] \geq \log(B-1) - I(\hat{\mathbf{Z}}; Y), \quad (19)$$

and thus minimizing $\mathcal{L}_{contrast}$ maximizes a lower bound of $I(\hat{\mathbf{Z}}; Y)$. Increasing B raises $\log(B-1)$, thereby strengthening this lower bound and enhancing performance by preserving more task-relevant information. Although the derived bound can be loose with a small number of negative samples [17], we mitigate this by sampling large batches (2048) during contrastive training.

B. Reconstruction for Task-Irrelevant Features

To maximize $I(\hat{Z}_2; X|Y)$, we use a reconstruction-based objective that ensures X is reconstructed from both Y and \hat{Z}_2 , where \hat{Z}_2 captures the information in X that is not already captured by Y . Let $g_\eta: \mathbb{R}^N \rightarrow \mathbb{R}^d$ represent the task-irrelevant encoder, parameterized by η , which maps input $\mathbf{x} \in \mathbb{R}^N$ to encoded task-irrelevant representation $\hat{\mathbf{z}}_2 \in \mathbb{R}^d$. The encoder approximates the posterior distribution of the latent variable $\hat{\mathbf{z}}_2$ given \mathbf{x} , which we denote by $q(\hat{\mathbf{z}}_2|\mathbf{x})$. This encoder is responsible for capturing features unrelated to the task, i.e., the features not directly useful for predicting \mathbf{y} . Mathematically, the encoded task-irrelevant representation is given by

$$\hat{\mathbf{z}}_2 = g_\eta(\mathbf{x}), \quad (20)$$

where d represents the dimensionality of the task-irrelevant feature space.

Next, we introduce the reconstructor $r_\omega: \mathbb{R}^d \times \mathbb{R}^M \rightarrow \mathbb{R}^N$, parameterized by ω . The reconstructor r_ω takes as input both noisy task-irrelevant features $\hat{\mathbf{z}}_2$ and task-relevant label \mathbf{y} and attempts to reconstruct the original input \mathbf{x} . The objective is to minimize the reconstruction error, ensuring that $\hat{\mathbf{z}}_2$ focuses solely on task-irrelevant information. The reconstruction loss is defined as

$$\mathcal{L}_{\text{recon}} = \mathbb{E}_{p(\mathbf{x}, \mathbf{y})} [\|r_\omega(\hat{\mathbf{z}}_2, \mathbf{y}) - \mathbf{x}\|^2]. \quad (21)$$

To justify this approach, we show how this reconstruction-based loss provides an approximation for the mutual information $I(\hat{Z}_2; X|Y)$. Using a variational encoder and reconstruction model $r_\omega(\mathbf{x}|\hat{\mathbf{z}}_2, \mathbf{y})$, we can approximate $I(\hat{Z}_2; X|Y)$ as follows,

$$I(\hat{Z}_2; X|Y) \geq \mathbb{E}_{p(\mathbf{x}, \mathbf{y})q(\hat{\mathbf{z}}_2|\mathbf{x})} [\log p(\mathbf{x}|\mathbf{y}, \hat{\mathbf{z}}_2)] - \mathbb{E}_{p(\mathbf{x}, \mathbf{y})} [\log p(\mathbf{x}|\mathbf{y})]. \quad (22)$$

The first term, $\mathbb{E}_{p(\mathbf{x}, \mathbf{y})q(\hat{\mathbf{z}}_2|\mathbf{x})} [\log p(\mathbf{x}|\mathbf{y}, \hat{\mathbf{z}}_2)]$, represents the expected log-likelihood of reconstructing \mathbf{x} given both \mathbf{y} and $\hat{\mathbf{z}}_2$. The second term, $\mathbb{E}_{p(\mathbf{x}, \mathbf{y})} [\log p(\mathbf{x}|\mathbf{y})]$, represents the expected log-likelihood of reconstructing \mathbf{x} based solely on \mathbf{y} , independent of the task-irrelevant features.

Minimizing the reconstruction loss $\mathcal{L}_{\text{recon}}$ effectively approximates the maximization of the first term in the mutual information expression, thereby increasing $I(\hat{Z}_2; X|Y)$. By optimizing both the encoder g_η and the reconstructor r_ω , we ensure that $\hat{\mathbf{z}}_2$ captures task-irrelevant information while leveraging \mathbf{y} for the reconstruction of task-relevant features in \mathbf{x} .

C. Adversarial Disentanglement

To approximate the minimization of the mutual information $I(\hat{Z}_1; \hat{Z}_2)$, we employ adversarial training, following the approach in [27]. This ensures that task-relevant features in \hat{Z}_1 and task-irrelevant features in \hat{Z}_2 are disentangled. The mutual information $I(\hat{Z}_1; \hat{Z}_2)$ quantifies the dependence between \hat{Z}_1 and \hat{Z}_2 . It is formally defined as

$$I(\hat{Z}_1; \hat{Z}_2) = \int_{\hat{\mathbf{z}}_1} \int_{\hat{\mathbf{z}}_2} p(\hat{\mathbf{z}}_1, \hat{\mathbf{z}}_2) \log \left(\frac{p(\hat{\mathbf{z}}_1, \hat{\mathbf{z}}_2)}{p(\hat{\mathbf{z}}_1)p(\hat{\mathbf{z}}_2)} \right) d\hat{\mathbf{z}}_1 d\hat{\mathbf{z}}_2. \quad (23)$$

Minimizing it promotes independence between these two representations. However, directly computing $I(\hat{Z}_1; \hat{Z}_2)$ is intractable since it requires access to the underlying joint distribution $p(\hat{\mathbf{z}}_1, \hat{\mathbf{z}}_2)$ and the product of the marginals $p(\hat{\mathbf{z}}_1)p(\hat{\mathbf{z}}_2)$. To circumvent this, we approximate the minimization using a discriminator to distinguish between samples drawn from the joint distribution $p(\hat{\mathbf{z}}_1, \hat{\mathbf{z}}_2)$ and samples drawn from the product of the marginals $p(\hat{\mathbf{z}}_1)p(\hat{\mathbf{z}}_2)$.

To approximate the joint distribution, we sample pairs $(\hat{\mathbf{z}}_1, \hat{\mathbf{z}}_2)$ from the encoder's output for the same input data point, which represents samples from $p(\hat{\mathbf{z}}_1, \hat{\mathbf{z}}_2)$. For the marginal distribution, we shuffle $\hat{\mathbf{z}}_2$ across the batch, generating $(\hat{\mathbf{z}}_1, \hat{\mathbf{z}}'_2)$, where $\hat{\mathbf{z}}'_2$ is a shuffled version of $\hat{\mathbf{z}}_2$ from a different data point. This ensures that $\hat{\mathbf{z}}_1$ and $\hat{\mathbf{z}}'_2$ are independent, approximating the product of the marginals $p(\hat{\mathbf{z}}_1)p(\hat{\mathbf{z}}_2)$. Let D_ν represent the discriminator parameterized by ν , trained to distinguish between joint samples $(\hat{\mathbf{z}}_1, \hat{\mathbf{z}}_2)$ and marginal samples $(\hat{\mathbf{z}}_1, \hat{\mathbf{z}}'_2)$. The adversarial loss is defined as

$$\mathcal{L}_{\text{adv}} = \mathbb{E}_{p(\hat{\mathbf{z}}_1, \hat{\mathbf{z}}_2)} [\log D_\nu(\hat{\mathbf{z}}_1, \hat{\mathbf{z}}_2)] + \mathbb{E}_{p(\hat{\mathbf{z}}_1)p(\hat{\mathbf{z}}_2)} [\log (1 - D_\nu(\hat{\mathbf{z}}_1, \hat{\mathbf{z}}'_2))]. \quad (24)$$

This loss encourages D_ν to assign high probabilities to true joint samples $(\hat{\mathbf{z}}_1, \hat{\mathbf{z}}_2)$ and low probabilities to independent (shuffled) samples $(\hat{\mathbf{z}}_1, \hat{\mathbf{z}}'_2)$.

To promote disentanglement in the encoder, we add an adversarial penalty to the encoder's loss. The encoder is trained to fool the discriminator by making the joint distribution $p(\hat{\mathbf{z}}_1, \hat{\mathbf{z}}_2)$ indistinguishable from the product of the marginals $p(\hat{\mathbf{z}}_1)p(\hat{\mathbf{z}}_2)$. The encoder's loss for disentanglement is defined as

$$\mathcal{L}_{\text{enc}} = \mathbb{E}_{p(\hat{\mathbf{z}}_1, \hat{\mathbf{z}}_2)} [\log (1 - D_\nu(\hat{\mathbf{z}}_1, \hat{\mathbf{z}}_2))]. \quad (25)$$

Minimizing \mathcal{L}_{enc} encourages the encoder to make $\hat{\mathbf{z}}_1$ and $\hat{\mathbf{z}}_2$ as independent as possible, thereby minimizing the mutual information $I(\hat{Z}_1; \hat{Z}_2)$. This ensures that the latent representations $\hat{\mathbf{z}}_1$ and $\hat{\mathbf{z}}_2$ are disentangled, with $\hat{\mathbf{z}}_1$ capturing task-relevant information and $\hat{\mathbf{z}}_2$ capturing task-irrelevant information.

D. Classification Task

The final downstream task is classification, where the goal is to predict the label Y from the encoded features \hat{Z}_1 . We use a simple feed-forward neural network classifier $q_\phi(\mathbf{y}|\hat{\mathbf{z}}_1)$, parameterized by ϕ , and trained with a cross-entropy loss. The classifier takes as input the task-relevant features $\hat{\mathbf{z}}_1$ and is optimized to minimize the following cross-entropy loss:

$$\mathcal{L}_{\text{class}} = -\mathbb{E}_{p(\mathbf{x}, \mathbf{y})} \left[\sum_{c=1}^C y_c \log q_\phi(y_c|\hat{\mathbf{z}}_1) \right], \quad (26)$$

where C is the number of classes, and y_c is the ground truth one-hot encoded label for class c .

E. Training Procedure

Training a complex system with many different components and loss function must be performed carefully to ensure that

Algorithm 2 Stage 2: Train Task-Relevant Encoder with Contrastive Loss and Discriminator

Input: \mathcal{X}_{train} (Training dataset), g_η (Task-irrelevant encoder), λ (Learning rate), λ_{adv} (Discriminator learning rate), κ (SNR), τ (Temperature)

Output: f_θ

- 1: Initialize θ, ψ, ν
- 2: **while** not converged **do**
- 3: $(\mathbf{x}, \mathbf{y}) \sim \mathcal{X}_{train}$
- 4: $\tilde{\mathbf{x}}_1 \leftarrow \text{Augment}(\mathbf{x}), \tilde{\mathbf{x}}_2 \leftarrow \text{Augment}(\mathbf{x})$
- 5: $\mathbf{z}_1^{(1)} \leftarrow f_\theta(\tilde{\mathbf{x}}_1), \mathbf{z}_1^{(2)} \leftarrow f_\theta(\tilde{\mathbf{x}}_2)$
- 6: $\mathbf{n}_1 \sim \mathcal{N}(0, \sigma^2 \mathbf{I}), \sigma^2 \leftarrow \frac{\mathbb{E}[\|\mathbf{z}_1\|^2]}{10^{\frac{\kappa}{10}}}$
- 7: $\mathbf{n}_2 \sim \mathcal{N}(0, \sigma^2 \mathbf{I}), \sigma^2 \leftarrow \frac{\mathbb{E}[\|\mathbf{z}_2\|^2]}{10^{\frac{\kappa}{10}}}$
- 8: $\hat{\mathbf{z}}_1^{(1)} \leftarrow \mathbf{z}_1^{(1)} + \mathbf{n}_1, \hat{\mathbf{z}}_1^{(2)} \leftarrow \mathbf{z}_1^{(2)} + \mathbf{n}_1$
- 9: $\mathbf{h}_1 \leftarrow h_\psi(\hat{\mathbf{z}}_1^{(1)}), \mathbf{h}_2 \leftarrow h_\psi(\hat{\mathbf{z}}_1^{(2)})$
- 10: $\mathcal{L}_{contrast} \leftarrow \text{Contrastive Loss}(\mathbf{h}_1, \mathbf{h}_2, \tau)$
- 11: $\theta \leftarrow \theta - \lambda \nabla_\theta \mathcal{L}_{contrast}$
- 12: $\psi \leftarrow \psi - \lambda \nabla_\psi \mathcal{L}_{contrast}$
- 13: $\mathbf{z}_1 \leftarrow f_\theta(\mathbf{x}), \mathbf{z}_2 \leftarrow g_\eta(\mathbf{x})$
- 14: $\hat{\mathbf{z}}_1 \leftarrow \mathbf{z}_1 + \mathbf{n}_1, \hat{\mathbf{z}}_2 \leftarrow \mathbf{z}_2 + \mathbf{n}_2$
- 15: $\hat{\mathbf{z}}_2' \leftarrow \text{Shuffle } \hat{\mathbf{z}}_2 \text{ across the batch}$
- 16: $\mathcal{L}_{adv} \leftarrow \log D_\nu(\hat{\mathbf{z}}_1, \hat{\mathbf{z}}_2) + \log(1 - D_\nu(\hat{\mathbf{z}}_1, \hat{\mathbf{z}}_2'))$
- 17: $\nu \leftarrow \nu - \lambda_{adv} \nabla_\nu \mathcal{L}_{adv}$
- 18: $\mathcal{L}_{enc} \leftarrow \log(1 - D_\nu(\hat{\mathbf{z}}_1, \hat{\mathbf{z}}_2))$
- 19: $\theta \leftarrow \theta - \lambda \nabla_\theta \mathcal{L}_{enc}$
- 20: **end while**
- 21: Discard h_ψ, D_ν, g_η
- 22: Freeze θ

Algorithm 3 Stage 3: Train Classifier on Frozen Task-Relevant Encoder

Input: \mathcal{X}_{train} (Training dataset), f_θ (Task relevant encoder), learning rate λ, κ (SNR)

Output: Trained classifier q_ϕ

- 1: Initialize ϕ
- 2: **while** not converged **do**
- 3: Sample $(\mathbf{x}, \mathbf{y}) \sim \mathcal{X}_{train}$
- 4: $\mathbf{z}_1 \leftarrow f_\theta(\mathbf{x})$
- 5: $\mathbf{n} \sim \mathcal{N}(0, \sigma^2 \mathbf{I}), \sigma^2 \leftarrow \frac{\mathbb{E}[\|\mathbf{z}_1\|^2]}{10^{\frac{\kappa}{10}}}$
- 6: $\hat{\mathbf{z}}_1 \leftarrow \mathbf{z}_1 + \mathbf{n}$
- 7: $\hat{\mathbf{y}} \leftarrow q_\phi(\hat{\mathbf{z}}_1)$
- 8: $\mathcal{L}_{class} \leftarrow -\sum_{i=1}^C y_i \log \hat{y}_i$
- 9: $\phi \leftarrow \phi - \lambda \nabla_\phi \mathcal{L}_{class}$
- 10: **end while**

each stage achieves its goal without interfering with other objectives and that the gradients flow appropriately. The training is done in multiple stages, each targeting a different part of the system. Below, we outline the step-by-step procedure used to train our model and the associated algorithms.

Stage 1: Training the Task-Irrelevant Encoder: In the first stage, we train the task-irrelevant encoder g_η by pairing it with a reconstructor r_ω . The reconstructor r_ω learns to reconstruct an image by using the encoded representations from g_η as well as the label information. This encourages g_η to focus on capturing the parts of the input that are not

necessary for the downstream classification task by minimizing the reconstruction loss. The reconstructor is discarded, and the parameters of g_η are frozen after training to preserve the task-irrelevant features for later use. This procedure is outlined in Algorithm 1.

Stage 2: Training the Task-Relevant Encoder with Contrastive Loss and Discriminator: After freezing g_η , the task-relevant encoder f_θ is trained in this stage. We use both a contrastive loss to ensure that f_θ captures class-discriminative features and an adversarial loss to enforce disentanglement between the task-relevant encoder f_θ feature vector and the task-irrelevant encoder g_η feature vector. The task-relevant encoder is trained using augmented views of the input for contrastive learning and through adversarial training with the discriminator D_ν . The training process alternates between updating the contrastive loss and updating the discriminator and encoder to ensure disentanglement. The details of this stage are described in Algorithm 2.

Stage 3: Training the Classifier on the Frozen Task-Relevant Encoder: Once disentanglement is achieved, we discard the projection head h_ψ , the discriminator D_ν , and the task-irrelevant encoder g_η , leaving only the frozen task-relevant encoder f_θ . In this final stage, we train the classifier q_ϕ on top of f_θ for the downstream classification task. The classifier is trained with the cross-entropy loss, ensuring that it can utilize the task-relevant features f_θ for accurate classification. The classifier training procedure is outlined in Algorithm 3.

The separation of training stages is for stability, and also reflects a modular decomposition of the CLAD objective. Each stage isolates the gradient flow to the component most relevant for that term, making the multi-stage training strategy a practical approximation to optimizing \mathcal{L}_{CLAD} holistically.

F. Information Retention Index Across Different Methods

To assess how much information \hat{Z} retains about input X , we estimate $I(\hat{Z}; X)$, which quantifies the informativeness of the latent representation \hat{Z} for reconstructing the original input X . Since direct computation of mutual information is intractable, we adopt a reconstruction-based proxy [34] to compute the IRI across different methods.

Assume that the reconstruction loss $\mathcal{L}_{recon}(\mathbf{x}|\hat{\mathbf{z}})$, parameterized by a reconstructor $r_\gamma(\cdot)$ with parameters γ , denotes the expected error for reconstructing \mathbf{x} from the latent representation $\hat{\mathbf{z}}$. The mutual information $I(\hat{Z}; X)$ can be bounded as follows:

$$I(\hat{Z}; X) = H(X) - H(X|\hat{Z}) \geq H(X) - \mathbb{E}_{p(\mathbf{x}, \hat{\mathbf{z}})} [\mathcal{L}_{recon}(\mathbf{x}|\hat{\mathbf{z}})], \quad (27)$$

where $H(X)$ represents the entropy of the input, and $\mathcal{L}_{recon}(\mathbf{x}|\hat{\mathbf{z}})$ is the reconstruction loss. Therefore, one can compute $I(\hat{Z}; X)$ by minimizing the reconstruction error as follows:

$$I(\hat{Z}; X) \geq H(X) - \min_{\gamma} \mathcal{L}_{recon}^{\gamma}(\mathbf{x}|\hat{\mathbf{z}}). \quad (28)$$

In practice, for each task-oriented communication method we evaluate, the corresponding encoder parameters are frozen, and a reconstructor r_γ is trained to minimize the reconstruction loss $\mathcal{L}_{recon}(\mathbf{x}|\hat{\mathbf{z}})$. The reconstructor is trained using mean

squared error (MSE) as the loss function, and we evaluate the quality of the reconstructions using the structural similarity index measure (SSIM) [35]. SSIM serves as a proxy for the total mutual information between the input and the representation and can indicate the amount of encoded pixel-level information. It has been shown empirically that SSIM correlated with mutual information [34]. We drop $H(X)$ from our calculations as it is a constant.

Unlike MSE, which only measures pixel-wise differences, SSIM accounts for luminance, contrast, and structural information, providing a better perceptual measure of image quality. This makes SSIM a suitable proxy to indicate how much useful information from X is retained in \hat{Z} . The SSIM between two images x and \hat{x} is given by

$$\text{SSIM}(x, \hat{x}) = \frac{(2\mu_x\mu_{\hat{x}} + c_1)(2\sigma_{x\hat{x}} + c_2)}{(\mu_x^2 + \mu_{\hat{x}}^2 + c_1)(\sigma_x^2 + \sigma_{\hat{x}}^2 + c_2)}, \quad (29)$$

where μ_x and $\mu_{\hat{x}}$ are the mean intensities of the original and reconstructed images, σ_x^2 and $\sigma_{\hat{x}}^2$ are their variances, and $\sigma_{x\hat{x}}$ is the covariance between them. The constants c_1 and c_2 stabilize the division to avoid near-zero values.

The SSIM has a range from -1 and 1, with values closer to 1 indicating higher structural similarity. By focusing on perceptual quality rather than pixel-wise differences, we find that SSIM provides a more accurate measure of the retained information in the latent representation. Formally, we define the IRI for a given task-oriented communication system i as

$$\text{IRI}_i = \text{SSIM}(x, r_{\gamma_i}(\hat{z})), \quad (30)$$

where r_{γ_i} refers to the reconstructor specifically trained for system i .

To compare the different systems fairly, we ensure the following conditions:

- The same decoder architecture is used for each system, ensuring consistency across the experiments.
- All reconstructors are trained with the same settings and hyperparameters for the same number of epochs.
- We train all reconstructors on the same training set and to ensure a valid comparison, we assess the reconstruction performance on the same testing set.

By comparing the IRI scores on the reconstructed images, we can capture the information retention across different methods. The higher the IRI, the more information Z retains about X , allowing us to quantify the informativeness and minimality of the learned representations. Algorithm 4 provides a detailed procedure to compute the IRI by leveraging the correlation between reconstructed and original inputs to approximate informativeness and minimality.

While methods such as MINE [36] offer tighter approximations of MI, they require adversarial or variational training, are sensitive to hyperparameters, and are not directly comparable across model architectures. In contrast, IRI allows for consistent, fair benchmarking with minimal assumptions and training overhead. We view IRI as a relative measure, similar to a diagnostic tool, that enables empirical analysis of minimality and informativeness in task-oriented systems. We note that while SSIM is effective for evaluating visual similarity in

image-based applications, it is inherently limited to image data. For non-visual modalities such as text or tabular data, alternative reconstruction-based metrics (e.g., BLEU score) can be adopted to extend the IRI framework to broader task domains.

Algorithm 4 Computing IRI

Input: $\mathcal{X}_{train}, \mathcal{X}_{test}$ frozen encoders $\{f_{\theta_i}\}_{i=1}^M$, learning rate λ , κ (SNR)

Output: IRI for each system i

```

1: Initialize reconstructors  $\{r_{\gamma_i}\}_{i=1}^M$ 
2: for  $i = 1$  to  $M$  do
3:   Freeze  $\theta_i$ 
4:   while not converged do
5:     Sample  $(x, y) \sim \mathcal{X}_{train}$ 
6:      $z \leftarrow f_{\theta_i}(x)$ 
7:      $n \sim \mathcal{N}(0, \sigma^2 \mathbf{I})$ ,  $\sigma^2 \leftarrow \frac{\mathbb{E}[\|z_1\|^2]}{10^{\frac{\kappa}{10}}}$ 
8:      $\hat{z}_1 \leftarrow z_1 + n$ 
9:      $\hat{x} \leftarrow r_{\gamma_i}(\hat{z}_1)$ 
10:     $\mathcal{L}_{recon} \leftarrow \|x - \hat{x}\|^2$ 
11:     $\gamma_i \leftarrow \gamma_i - \lambda_{rec} \nabla_{\gamma_i} \mathcal{L}_{recon}$ 
12:   end while
13: end for
14: for  $i = 1$  to  $M$  do
15:   Sample  $(x, y) \sim \mathcal{X}_{test}$ 
16:    $z \leftarrow f_{\theta_i}(x)$ 
17:    $n \sim \mathcal{N}(0, \sigma^2 \mathbf{I})$ ,  $\sigma^2 \leftarrow \frac{\mathbb{E}[\|z_1\|^2]}{10^{\frac{\kappa}{10}}}$ 
18:    $\hat{z}_1 \leftarrow z_1 + n$ 
19:    $\hat{x} \leftarrow r_{\gamma_i}(\hat{z}_1)$ 
20:    $\text{IRI}_i \leftarrow \text{SSIM}(x, \hat{x})$ 
21: end for

```

VI. EXPERIMENTAL EVALUATIONS AND DISCUSSION

In this section, we present the experimental setup used to evaluate CLAD. We start by describing the datasets used in our experiments, followed by a discussion of the baseline methods, neural architectures, and the experimental setup. Finally, we present detailed evaluations and analysis of the results.¹

A. Experimental Setup

1) *Datasets:* The Colored MNIST and Colored FashionMNIST datasets are extensions of the standard MNIST [37] and FashionMNIST [38] datasets, each consisting of 60,000 28x28 grayscale images. In Colored MNIST, handwritten digits (0-9) are overlaid on colored backgrounds, while in Colored FashionMNIST, clothing items from 10 categories (e.g., T-shirts, coats, shoes) are similarly displayed on colored backgrounds. The introduction of background colors adds additional task-irrelevant information, creating a more challenging setup for the model to disentangle task-relevant features relevant to classifying digits or clothing items from background-related attributes. Furthermore, incorporating background color labels enables the evaluation of attribute inference attacks, where an

¹The source code, models and results are available at <https://github.com/OmarErak/CLAD>

adversary is trained to predict background color. This setup provides insight into the model’s ability to protect against such attacks while maintaining disentanglement between task-relevant and task-irrelevant features. To further evaluate the scalability and robustness of the proposed method on more complex and natural datasets, we also incorporate CIFAR-10 [?]. CIFAR-10 consists of 60,000 32x32 color images in 10 classes, including airplanes, cars, birds, cats, and other natural objects. Compared to MNIST-based datasets, CIFAR-10 introduces significantly more visual variability and semantic richness, making it a more challenging benchmark.

2) *Neural Network Architectures*: In this work, we employ a deep neural network (DNN) architecture for the classification tasks across all datasets. These architectures consists of convolutional and fully connected layers, with a latent dimension $d = 64$. The architectures, detailed in Table I and Table III, serve as the backbone for the task-relevant encoder (transmitter) and the downstream classification task (receiver). The same architecture is used across all baselines to ensure a consistent and fair comparison of methods. To compute the IRI, for each method we train multiple reconstructors that aim to reconstruct the original input \mathbf{x} from the latent representation $\hat{\mathbf{z}}$. The reconstructor architectures are described in Table II and Table IV, and it is used consistently across all methods for IRI computations.

3) *Channel Conditions*: We evaluate the performance of CLAD compared to baseline methods using an AWGN channel model due to its widespread adoption and ease of use. Specifically, we consider training and testing the models at identical SNRs, ranging from -6 dB to 12 dB. This setting allows us to assess the robustness of each method across different noise levels in a controlled manner. For each SNR value, we train the models over multiple runs and average the results to mitigate any randomness introduced during training.

TABLE I. DNN Structure for the transmitter (encoder) and the receiver (classifier) used for Colored MNIST and FashionMNIST

	Layer	Output dimensions
Transmitter	Conv Layer+ReLU	32×28×28
	MaxPool Layer	32×14×14
	Conv Layer+ReLU	64×14×14
	MaxPool Layer	64×7×7
	Fully Connected (Flatten)	d
Receiver	Fully Connected (FC)	512
	Fully Connected (FC)	256
	Fully Connected + Softmax	10

B. Baselines

In our experiments, we compare the proposed method CLAD against two baselines: DeepJSCC [14] and Variational Information Bottleneck (VIB) [13], [16]. These methods provide a benchmark for task-oriented communication systems,

TABLE II. Architecture settings for the reconstructors used with Colored MNIST and FashionMNIST to evaluate IRI

	Layer name	Output dimensions
Reconstructor	Fully Connected (FC)	128×7×7
	Deconv Layer + ReLU	64×14×14
	Deconv Layer + ReLU	32×28×28
	Deconv Layer + ReLU	16×28×28
	Deconv Layer + Sigmoid	3×28×28

TABLE III. DNN structure for the transmitter (encoder) and the receiver (classifier) used for CIFAR-10

	Layer	Output Dimensions
Transmitter	Conv + ReLU ×2	128×32×32
	ResNet Block	128×16×16
	Conv + ReLU ×2	4×4×4
	Reshape + FC + Tanh	d
Receiver	FC + ReLU + Reshape	64×4×4
	Conv + ReLU ×2	512×4×4
	ResNet Block	512×4×4
	Pooling Layer	512
	FC + Softmax	10

helping to evaluate the effectiveness of our approach in disentangling task-relevant and task-irrelevant features, and improving predictive accuracy through contrastive learning.

1) *DeepJSCC*: DeepJSCC is a neural network-based approach that optimizes the encoding of data for transmission over noisy channels. For our task-oriented scenario, DeepJSCC is trained with cross-entropy loss for classification rather than reconstruction, and it does not explicitly discard task-irrelevant information. As a result, it serves as a baseline for how well the encoded representation performs without feature disentanglement.

2) *Variational Information Bottleneck (VIB)*: The variational information bottleneck (VIB) framework aims to compress the input X into latent representation Z while retaining sufficient information for predicting Y . VIB balances $I(Z; X)$ and $I(Z; Y)$ via hyperparameter β . In our experiments, we provide results for different values of β to illustrate how varying the trade-off between compression and task relevance impacts task performance, IRI, and privacy. The work in [13] is based on VIB, and therefore, we reproduce their results as a baseline comparison.

TABLE IV. Architecture settings for the reconstructors used with CIFAR-10 to evaluate IRI

	Layer name	Output dimensions
Reconstructor	Fully Connected (FC) + ReLU	512×4×4
	Deconv (512→256) + ReLU	256×8×8
	Deconv (256→128) + ReLU	128×16×16
	Deconv (128→64) + ReLU	64×32×32
	Conv (64→3) + Sigmoid	3×32×32

By comparing our method to these two baselines, we demonstrate how CLAD improves task-relevant feature extraction, minimizes task-irrelevant information, achieves better performance in downstream classification tasks and provides better privacy.

C. Evaluation Metrics

To evaluate the effectiveness of CLAD, we utilize three key metrics: task performance through classification accuracy, IRI, and attribute inference attack accuracy. These metrics provide insights into how well the method performs in terms of classification accuracy, information retention, and privacy awareness. Additionally, we assess all methods at different channel SNRs to measure performance under various dynamic transmission conditions.

1) *Task Performance (Accuracy)*: The primary evaluation metric for task performance is classification accuracy. It measures the ability of classifier to predict the label \mathbf{y} from $\hat{\mathbf{z}}$. Accuracy is calculated as the ratio of correctly classified instances to the total number of instances:

$$\text{Accuracy} = \frac{1}{N} \sum_{i=1}^N \mathbb{1}(\hat{y}_i = y_i), \quad (31)$$

where N is the total number of samples, \hat{y}_i is the predicted label, and y_i is the ground truth label.

2) *Information Retention Index (IRI)*: To quantify the amount of information retained in the encoded representation $\hat{\mathbf{Z}}$, we use our proposed method to compute the IRI. This measures how much information from the input X is present in the encoded representation $\hat{\mathbf{Z}}$, which helps assess the compression of the representation. By comparing IRI across different methods, we can evaluate how effectively each method discards task-irrelevant information.

3) *Attribute Inference Attack*: In addition to task performance and information retention, we also evaluate privacy by comparing the vulnerability of different methods to attribute inference attacks. An attribute inference attack aims to recover sensitive or irrelevant information about the input, such as background color, from the encoded representation $\hat{\mathbf{z}}$.

Given the encoded representation $\hat{\mathbf{z}}$, the adversary seeks to predict the background color of the image. If $\hat{\mathbf{z}}$ contains significant task-irrelevant information, the adversary will be able to classify the background color with high accuracy. To evaluate this, we train a background color classifier (with the same architecture as the task relevant classifier in Table I) on the encoded representation $\hat{\mathbf{z}}$ and report its classification accuracy. A higher accuracy in the attribute inference attack implies more task-irrelevant information is retained in $\hat{\mathbf{z}}$, indicating weaker privacy guarantees.

D. Results and Analysis

In this subsection we thoroughly analyze and discuss the performance of the proposed method CLAD against the two baselines, DeepJSCC and VIB, on all three aforementioned datasets.

TABLE V. Evaluation of different methods on Colored MNIST dataset at SNR = 12 dB.

Method	Classification Accuracy (%)	IRI	Adversarial Accuracy (%)
DeepJSCC	97.96	0.608	79.16
VIB (Beta=0.001)	97.90	0.1931	34.09
VIB (Beta=0.01)	96.93	0.0608	22.96
VIB (Beta=0.1)	93.29	0.0342	17.56
VIB (Beta=1)	11.36	0.0123	13.52
CLAD (Ours)	98.42	0.039	19.83

TABLE VI. Evaluation of different methods on Colored FashionMNIST dataset at SNR = 12 dB.

Method	Classification Accuracy (%)	IRI	Adversarial Accuracy (%)
DeepJSCC	89.28	0.5958	79.52
VIB (Beta=0.001)	89.30	0.2562	47.00
VIB (Beta=0.01)	86.98	0.0707	23.55
VIB (Beta=0.1)	81.82	0.0497	17.06
VIB (Beta=1)	11.28	0.0101	12.82
CLAD (Ours)	91.74	0.0587	19.33

1) *Colored MNIST Results*: Fig. 4a shows the accuracy as a function of the SNR for each method. Here, it is evident that CLAD outperforms all the baselines at different channel conditions. This is a strong indication that maximizing $I(\hat{\mathbf{Z}}; Y)$ through contrastive learning yields better feature extraction and classification performance, even with undesirable and high noise conditions. As seen in Table V, CLAD outperforms both DeepJSCC and VIB, achieving the highest classification accuracy of 98.42% at SNR = 12 dB. This represents a 0.46% improvement over DeepJSCC (97.96%) and a 0.52% improvement over VIB at $\beta = 0.001$ (97.90%). The higher accuracy of CLAD can be attributed to its ability to learn a more disentangled and task-relevant latent space using contrastive learning and adversarial disentanglement.

From Table V, CLAD achieves a very low IRI value of 0.039. TABLE VII. Evaluation of different methods on CIFAR10 dataset at SNR = 12 dB.

Method	Classification Accuracy (%)	IRI
DeepJSCC	91.21	0.2043
VIB (Beta=0.001)	91.49	0.1132
VIB (Beta=0.01)	86.42	0.0456
VIB (Beta=0.1)	78.31	0.0321
VIB (Beta=1)	9.67	0.0092
CLAD (Ours)	92.33	0.0471

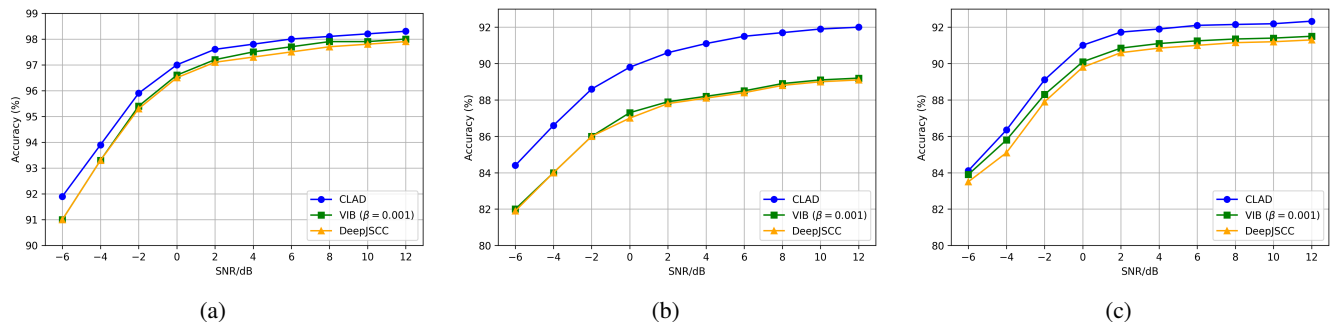


Figure 4. Accuracy at different SNRs for (a) the Colored MNIST dataset, (b) the Colored FashionMNIST dataset and (c) the CIFAR-10 dataset .

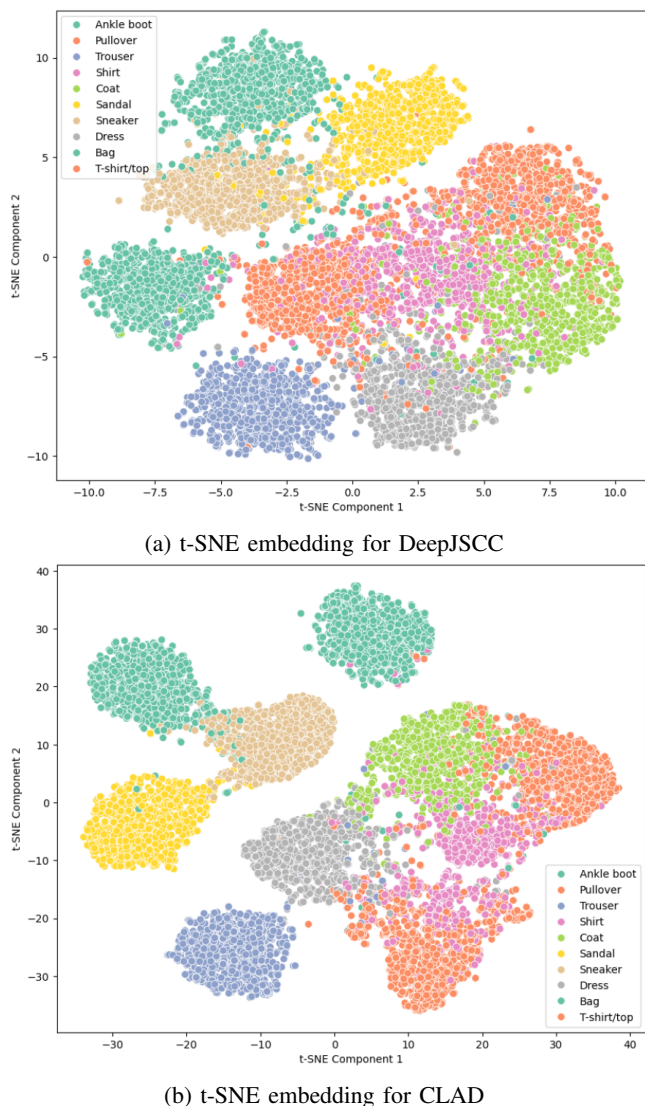


Figure 5. 2-dimensional t-SNE embeddings of the received feature representations for the Colored FashionMNIST classification task at SNR = 12 dB.

0.039, drastically outperforming DeepJSCC (0.608) and VIB at $\beta = 0.001$ (0.1931). This substantial difference shows that CLAD is effective at disentangling and removing task-irrelevant information from its encoded representations. This

is further supported by the significantly lower adversarial accuracy of CLAD compared to DeepJSCC and VIB at $\beta = 0.001$. From Fig. 6a, we can visually see that image reconstructions from CLAD excel in retaining task-relevant information and preserving the core structure of the digits while discarding irrelevant information such as background color and other style features such as thickness or slant in the digit. This contrasts with DeepJSCC and VIB, which retain unnecessary information such as background color and thickness and slant of the digit.

Interestingly, from Table V, VIB at lower β values (e.g., $\beta = 0.01$ and $\beta = 0.1$) achieves IRI values that are closer to CLAD. However, the major drawback of VIB is that, while it improves privacy, informativeness and minimality, it comes at the cost of accuracy, especially as β increases, as shown in the table. For example, at $\beta = 0.1$, VIB achieves even lower IRI, however its classification accuracy drops to 93.29%, which is significantly lower than both CLAD and DeepJSCC. This demonstrates that CLAD maintains task performance while better preserving accuracy compared to VIB.

2) *Colored FashionMNIST Results:* For the more challenging Colored FashionMNIST dataset, it is evident from Fig. 4b, that CLAD shows even greater improvements across all SNR levels, with performance gains of up to 3% at higher SNR levels compared to other baselines. This demonstrates that CLAD becomes even more useful and essential for more complex computer vision tasks. Additionally, we visualize the noisy feature vector from the Colored FashionMNIST classification task using a two-dimensional t-distributed stochastic neighbor embedding (t-SNE) [39] in Fig. 5. Since CLAD effectively captures task-relevant features through contrastive learning and discards task-irrelevant information, it produces better class separation compared to DeepJSCC, as observed in the clearer clustering of feature representations.

In Table VI CLAD outperforms DeepJSCC with a 2.46% improvement and VIB at $\beta = 0.001$ with 2.44% increase in accuracy. The IRI and adversarial accuracy results for Colored FashionMNIST reflect similar trends as observed in the Colored MNIST dataset. CLAD achieves a considerably lower IRI and lower adversarial accuracy compared to DeepJSCC and VIB at $\beta = 0.001$, further confirming that CLAD is better at disentangling task-irrelevant information and maintaining privacy awareness. Fig. 6b, visually illustrates the varying

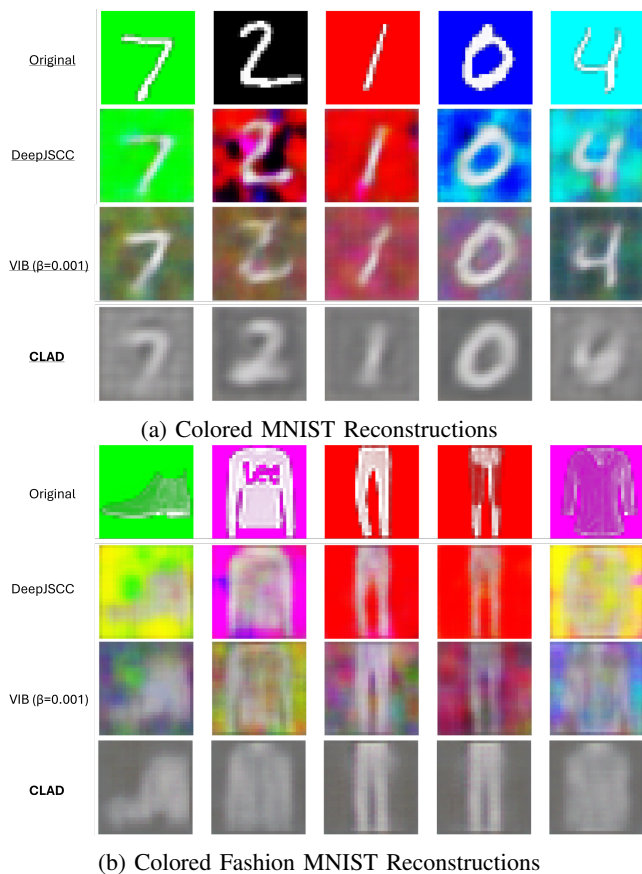


Figure 6. Reconstructed images from the received feature representations under different methods.

levels of informativeness and minimality in the encoded representations produced by each method, with respect to the input. In this image CLAD effectively removes most style features such as color, texture, and fine details, focusing solely on the basic shapes necessary for classification. For example, the CLAD reconstructions of the shoe, trousers, and shirt are reduced to simple grayscale silhouettes, discarding the vibrant colors and textures seen in the original and DeepJSCC versions. DeepJSCC retains style features such as color and subtle details such as the texture of fabric, making the reconstructions more complex but less focused on task-relevant information. VIB also retains some color and texture but introduces significant blurring, partially losing both class-relevant and style features. In contrast, CLAD’s grayscale, simplified images prioritize the task-relevant information necessary for downstream classification.

Once again, from Table VI, VIB achieves smaller IRI values at smaller β settings but suffers a drop in accuracy, and the IRI continues to decrease as β increases at the expense of even lower accuracy. This demonstrates that while VIB can be tuned to prioritize privacy and improve the minimality of the feature vector, it often struggles to maintain high classification performance.

3) *CIFAR-10 Results*: For the more complex CIFAR-10 dataset, Fig. 4c illustrates that CLAD continues to outperform baseline methods across all SNR levels. The performance gap becomes particularly notable at higher SNRs, where CLAD

achieves up to 2% improvement in classification accuracy over DeepJSCC and VIB.

As shown in Table VII, CLAD delivers the highest classification accuracy of 92.33% at 12 dB, outperforming DeepJSCC by 1.13% and VIB (with $\beta = 0.001$) by 0.84%. Moreover, CLAD achieves a significantly lower IRI compared to DeepJSCC, demonstrating its ability to retain task-relevant features while discarding redundant information, even in a dataset with rich visual complexity and no explicit sensitive attributes. These results reinforce CLAD’s robustness in encoding informative yet compact representations for more challenging computer vision tasks, without compromising classification performance.

VII. CONCLUSIONS

In this work, we have proposed a new task-oriented communication system, CLAD, based on contrastive learning and adversarial disentanglement. The proposed framework effectively disentangles task-relevant and task-irrelevant features, leading to enhanced performance in downstream tasks while simultaneously improving privacy as demonstrated using attribute inference attacks. Additionally, by disentangling task-relevant and task-irrelevant features, we reduce number of information bits that need to be transmitted. By leveraging contrastive learning, we enforce the model to capture discriminative task-relevant features, while adversarial disentanglement ensures that task-irrelevant features are separated, minimizing the mutual information between task-relevant and irrelevant representations. Furthermore, we present an approach to compute and compare the information retention between the input and encoded feature vectors across different methods, offering a practical and effective metric for the community to evaluate different task-oriented communication systems, which has been often neglected. Our results demonstrate that CLAD outperforms different state of the art task-oriented communication systems in terms of task performance, privacy, informativeness and minimality of the encoded feature representation. Future work can explore extending CLAD to handle different tasks or more complex multimodal data, such as video or audio streams, where task relevance might shift dynamically.

REFERENCES

- [1] C. E. Shannon, “A mathematical theory of communication,” *The Bell Syst. Tech. J.*, vol. 27, no. 3, pp. 379–423, 1948.
- [2] W. Saad, M. Bennis, and M. Chen, “A vision of 6G wireless systems: Applications, trends, technologies, and open research problems,” *IEEE Netw.*, vol. 34, no. 3, pp. 134–142, 2020.
- [3] M. Giordani, M. Polese, M. Mezzavilla, S. Rangan, and M. Zorzi, “Toward 6G networks: Use cases and technologies,” *IEEE Commun. Mag.*, vol. 58, no. 3, pp. 55–61, 2020.
- [4] A. Voulodimos, N. Doulamis, A. Doulamis, and E. Protopapadakis, “Deep learning for computer vision: A brief review,” *Comput. Intell. Neuroscience*, vol. 2018, no. 1, p. 7068349, 2018.
- [5] I. Yaqoob, L. U. Khan, S. A. Kazmi, M. Imran, N. Guizani, and C. S. Hong, “Autonomous driving cars in smart cities: Recent advances, requirements, and challenges,” *IEEE Netw.*, vol. 34, no. 1, pp. 174–181, 2019.
- [6] T. Andrade and D. Bastos, “Extended reality in iot scenarios: Concepts, applications and future trends,” in *2019 5th Experiment Int. Conf. (exp. at’19)*. IEEE, 2019, pp. 107–112.
- [7] L. Bariah, Q. Zhao, H. Zou, Y. Tian, F. Bader, and M. Debbah, “Large generative AI models for telecom: The next big thing?” *IEEE Commun. Mag.*, pp. 1–7, 2024.

- [8] D. Gündüz, Z. Qin, I. Estella Aguerri, H. S. Dhillon, Z. Yang, A. Yener, K. K. Wong, and C.-B. Chae, "Guest editorial special issue on beyond transmitting bits: Context, semantics, and task-oriented communications," *IEEE J. Sel. Areas Commun.*, vol. 41, no. 1, pp. 1–4, 2023.
- [9] Y. Shi, Y. Zhou, D. Wen, Y. Wu, C. Jiang, and K. B. Letaief, "Task-oriented communications for 6G: Vision, principles, and technologies," *IEEE Wireless Commun.*, vol. 30, no. 3, pp. 78–85, 2023.
- [10] Y. Mehmood, F. Ahmad, I. Yaqoob, A. Adnane, M. Imran, and S. Guizani, "Internet-of-things-based smart cities: Recent advances and challenges," *IEEE Commun. Mag.*, vol. 55, no. 9, pp. 16–24, 2017.
- [11] Q. Mao, F. Hu, and Q. Hao, "Deep learning for intelligent wireless networks: A comprehensive survey," *IEEE Commun. Surv. Tut.*, vol. 20, no. 4, pp. 2595–2621, 2018.
- [12] O. Erak and H. Abou-Zeid, "Accelerating and compressing deep neural networks for massive mimo csi feedback," in *ICC 2023-IEEE International Conference on Communications*. IEEE, 2023, pp. 1029–1035.
- [13] J. Shao, Y. Mao, and J. Zhang, "Learning task-oriented communication for edge inference: An information bottleneck approach," *IEEE J. Sel. Areas Commun.*, vol. 40, no. 1, pp. 197–211, 2021.
- [14] E. Boursoulatte, D. B. Kurka, and D. Gündüz, "Deep joint source-channel coding for wireless image transmission," *IEEE Trans. Cogn. Commun. Netw.*, vol. 5, no. 3, pp. 567–579, 2019.
- [15] S. Xie, S. Ma, M. Ding, Y. Shi, M. Tang, and Y. Wu, "Robust information bottleneck for task-oriented communication with digital modulation," *IEEE J. Sel. Areas Commun.*, vol. 41, no. 8, pp. 2577–2591, 2023.
- [16] A. A. Alemi, I. Fischer, J. V. Dillon, and K. Murphy, "Deep variational information bottleneck," in *Proc. Int. Conf. Learn. Represent.*, 2017.
- [17] A. v. d. Oord, Y. Li, and O. Vinyals, "Representation learning with contrastive predictive coding," *arXiv preprint arXiv:1807.03748*, 2018.
- [18] B. Paige, J.-W. Van De Meent, A. Desmaison, N. Goodman, P. Kohli, F. Wood, P. Torr *et al.*, "Learning disentangled representations with semi-supervised deep generative models," *Proc. Adv. Neural Inf. Process. Syst.*, vol. 30, 2017.
- [19] N. Tishby, F. C. Pereira, and W. Bialek, "The information bottleneck method," *arXiv preprint physics/0004057*, 2000.
- [20] M. Fredrikson, S. Jha, and T. Ristenpart, "Model inversion attacks that exploit confidence information and basic countermeasures," in *Proc. ACM SIGSAC Conf. Comput. Commun. Secur.*, 2015, pp. 1322–1333.
- [21] T. Chen, S. Kornblith, M. Norouzi, and G. Hinton, "A simple framework for contrastive learning of visual representations," in *Proc of the 37th Int. Conf. Mach. Learn.*, 2020.
- [22] Y. Tian, C. Sun, B. Poole, D. Krishnan, C. Schmid, and P. Isola, "What makes for good views for contrastive learning?" *Proc. Adv. Neural Inf. Process. Syst.*, vol. 33, pp. 6827–6839, 2020.
- [23] T. Chen, S. Kornblith, K. Swersky, M. Norouzi, and G. E. Hinton, "Big self-supervised models are strong semi-supervised learners," *Proc. Adv. Neural Inf. Process. Syst.*, vol. 33, pp. 22 243–22 255, 2020.
- [24] P. Khosla, P. Teterwak, C. Wang, A. Sarna, Y. Tian, P. Isola, A. Maschinot, C. Liu, and D. Krishnan, "Supervised contrastive learning," *Proc. Adv. Neural Inf. Process. Syst.*, vol. 33, pp. 18 661–18 673, 2020.
- [25] I. Higgins, L. Matthey, A. Pal, C. P. Burgess, X. Glorot, M. M. Botvinick, S. Mohamed, and A. Lerchner, "beta-vae: Learning basic visual concepts with a constrained variational framework," *Proc. Int. Conf. Learn. Representations (Poster)*, vol. 3, 2017.
- [26] H. Kim and A. Mnih, "Disentangling by factorising," in *Proc. Int. Conf. Mach. Learn.*, 2018, pp. 2649–2658.
- [27] E. H. Sanchez, M. Serrurier, and M. Ortner, "Learning disentangled representations via mutual information estimation," in *Proc. ECCV*. Springer, 2020, pp. 205–221.
- [28] Z. Pan, L. Niu, J. Zhang, and L. Zhang, "Disentangled information bottleneck," in *Proc. AAAI*, vol. 35, no. 10, 2021, pp. 9285–9293.
- [29] L. Sun, Y. Yang, M. Chen, and C. Guo, "Disentangled information bottleneck guided privacy-protective joint source and channel coding for image transmission," *IEEE Trans. Commun.*, pp. 1–1, 2024.
- [30] I. Goodfellow, J. Pouget-Abadie, M. Mirza, B. Xu, D. Warde-Farley, S. Ozair, A. Courville, and Y. Bengio, "Generative adversarial nets," *Proc. Adv. Neural Inf. Process. Syst.*, vol. 27, 2014.
- [31] I. Fischer, "The conditional entropy bottleneck," *Entropy*, vol. 22, no. 9, p. 999, 2020.
- [32] R. Shokri, M. Stronati, C. Song, and V. Shmatikov, "Membership inference attacks against machine learning models," in *Proc. IEEE Symp. Secur. Privacy (SP)*. IEEE, 2017, pp. 3–18.
- [33] R. Yeung, "A new outlook on shannon's information measures," *IEEE Trans. Inf. Theory*, vol. 37, no. 3, pp. 466–474, 1991.
- [34] R. D. Hjelm, A. Fedorov, S. Lavoie-Marchildon, K. Grewal, P. Bachman, A. Trischler, and Y. Bengio, "Learning deep representations by mutual information estimation and maximization," in *Proc. Int. Conf. Learn. Represent.*, 2019.
- [35] Z. Wang, A. C. Bovik, H. R. Sheikh, and E. P. Simoncelli, "Image quality assessment: from error visibility to structural similarity," *IEEE Trans. Image Process.*, vol. 13, no. 4, pp. 600–612, 2004.
- [36] M. I. Belghazi, A. Baratin, S. Rajeswar, S. Ozair, Y. Bengio, A. Courville, and R. D. Hjelm, "Mine: mutual information neural estimation," *arXiv preprint arXiv:1801.04062*, 2018.
- [37] L. Deng, "The MNIST database of handwritten digit images for machine learning research [best of the web]," *IEEE Signal Process. Mag.*, vol. 29, no. 6, pp. 141–142, 2012.
- [38] H. Xiao, K. Rasul, and R. Vollgraf, "Fashion-MNIST: a novel image dataset for benchmarking machine learning algorithms," 2017.
- [39] L. Van der Maaten and G. Hinton, "Visualizing data using t-SNE," *J. Mach. Learn. Res.*, vol. 9, no. 11, 2008.